Indian Journal of Biochemistry & Biophysics
Vol. 63, November 2026, pp. 1255-1268
DOI: 10.56042/ijbb.v63i11.22430

A Review

Structure-based design and computational screening of Fyn kinase inhibitors targeting neurodegenerative pathways in Alzheimer's disease

Ankit Ganeshpurkar[1]*, Dileep Kumar[2], Qadir Alam[3], Aditya Ganeshpurkar[4]*, Umesh Kumar Patil[1] & Devendra Kumar[5]

[1]Department of Pharmaceutical Sciences, Dr. Harisingh Gour Vishwavidyalaya (A Central University), Sagar-470 003, Madhya Pradesh, India

[2]Department of Pharmaceutical Chemistry, Manipal College of Pharmaceutical Sciences, Manipal Academy of Higher Education (MAHE), Manipal- 576 104, Karnataka, India

[3]Central Ayurveda Research Institute-CCRAS, Ministry of Ayush, Kolkata-700 091, West Bengal, India

[4]Shri Ram Institute of Technology-Pharmacy, Jabalpur-482 002, Madhya Pradesh, India

[5]School of Pharmacy & Technology Management, SVKM's NMIMS University, Shirpur-425 405, Maharashtra, India

Received 06 August 2025; *revised 30 October 2026*

Fyn kinase, a non-receptor tyrosine kinase, plays a crucial role in various cellular processes and is implicated in diseases like neurodegenerative disorders and cancer. The present study employed a structure-based virtual screening approach utilising a pharmacophore model derived from the known inhibitor staurosporine to identify potential therapeutic agents. MolPort, a large chemical database, was screened to obtain 1,127 initial hits, which were filtered based on drug-likeness, PAINS, pharmacokinetic properties, and toxicity profiles, resulting in 104 promising compounds.

Molecular docking of these compounds against the Fyn kinase ATP-binding site identified two top-ranking candidates, MolPort-000-414-107 and MolPort-005-915-880, exhibiting favourable binding energies and stable binding poses. To further evaluate the stability and dynamics of these interactions, 200 ns molecular dynamics simulations were performed. The simulations revealed that both ligands maintained stable binding within the Fyn kinase active site, with minimal RMSD fluctuations. Ligand binding led to a general reduction in protein flexibility and solvent accessibility. Hydrogen bond analysis highlighted distinct interaction patterns for each ligand, indicating different binding modes. MM-GBSA calculations predicted favourable binding free energies for both compounds, suggesting strong binding affinities. These *in silico* findings suggest that MolPort-000-414-107 and MolPort-005-915-880 are promising lead compounds for development of novel Fyn kinase inhibitors.

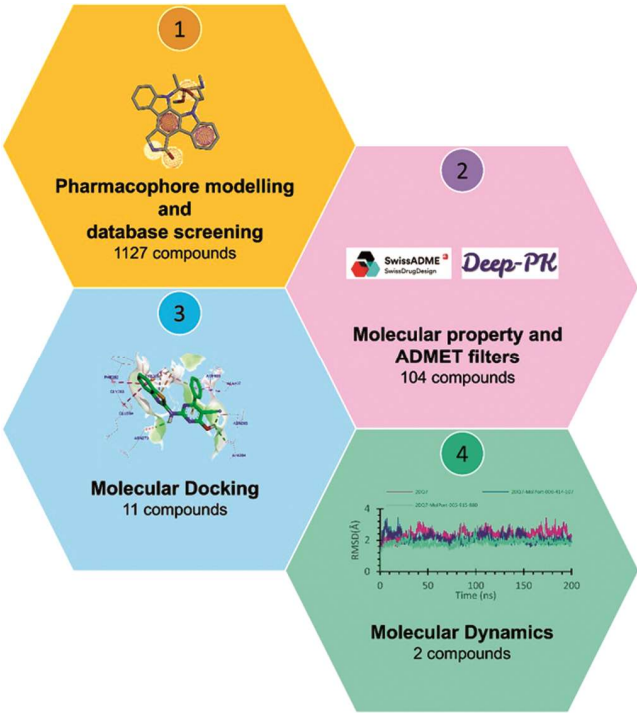
Keywords: Alzheimer's disease, Fyn kinase, Molecular docking, Molecular dynamics

Introduction

Tyrosine kinases (TKs) belong to the protein kinase enzyme group that catalyse the transfer of a phosphate group to tyrosine residues of substrate proteins from ATP. They regulate various signalling pathways involved in cell growth, differentiation, metabolism, immune responses, and neuronal plasticity[1]. Broadly, they are classified as receptor and cytoplasmic TKs[2]. These kinases show a conserved bilobed fold with distinct amino acid sequences and conformations responsible for characteristic differences in catalytic efficiency and specificity to substrate binding[3].

Fyn kinase is a non-receptor TK belonging to the Src family kinases (SFKs) localised in the cytoplasm and involved in various cellular processes. It is a 59 kDa protein with an N-terminal sequence, three modular SH domains (viz SH2, SH3 and kinase domains) and a C-terminal, each contributing to its regulatory and signalling functions[4]. The N-terminal region facilitates the anchoring of the kinase with the plasma membrane near its signalling partners. The SH2 domain enables the enzyme to recognise and bind to phosphorylated tyrosine residues on target proteins, mediating crucial protein–protein interactions for signal transduction. Further, the SH3 domain binds to proline-rich sequences, specifically PXXP motifs, thereby stabilising interactions with adaptor proteins[5]. The SH1 domain, or kinase domain, constitutes the catalytic core of Fyn kinase, responsible for phosphorylating downstream

*Correspondence:
E-mail: ankitganeshpurkar@gmail.com (AG);
adityaganeshpurkar@gmail.com (AG)
Suppl. data available on respective page of NOPR



Graphical abstract

substrates. Finally, the C-terminal tail contains regulatory tyrosine residues whose phosphorylation status modulates Fyn kinase activity, serving as a molecular switch for activation or inhibition. It is primarily localised in the 'cytoplasmic leaflet of the cell membrane' and phosphorylates the tyrosine residue of principal signalling proteins, modulating various cellular signalling pathways[6].

Staurosporine is a bisindole alkaloid initially isolated from *Streptomyces staurosporeus* in 1977[7]. It is an adenosine triphosphate (ATP) competitive inhibitor acting on a broad category of targets and does not compete for the peptide binding site. It inhibits protein kinase C, p60v-src, and protein kinase A at nonomolar IC_{50} concentrations[8,9]. On the other hand, casein kinase 1 (CK1), CK2, mitogen-activated protein kinase and C-terminal Src kinase (CSK) are inhibited at the micromolar range[10,11]. This differential potency, despite targeting the conserved ATP-binding site, reflects its selective affinity across various protein kinases.

Fyn kinase is a critical regulator implicated in cancer, neurodegeneration, autoimmune disorders, cardiovascular diseases, metabolic dysfunctions, and infectious diseases through its modulation of diverse signalling pathways. Fyn kinase plays a central role in the pathogenesis of Alzheimer's disease (AD) by contributing to both amyloid-β (Aβ)-induced neurotoxicity and tau pathology. Aβ oligomers interact with the cellular prion protein, which aberrantly activates Fyn kinase, resulting in synaptic dysfunction and excitotoxic neuronal damage. Further, it interacts with phosphorylated tau, promoting its hyperphosphorylation, aggregation, and the formation of neurofibrillary tangles[12]. In Fyn kinase deficient mouse models, a significant reduction in tau aggregation and neurofibrillary pathology has been observed. Moreover, pharmacological inhibition of Fyn kinase has demonstrated the ability to rescue synaptic and cognitive deficits and to reduce both Aβ- and tau-associated neurodegeneration[13]. These findings suggest that Fyn kinase is a significant therapeutic target, with ongoing clinical trials evaluating the efficacy of Fyn kinase inhibitors in mitigating AD-related neuropathology and cognitive decline[14,15].

Pharmacophore modelling, based on ligand interactions within the co-crystallized protein structure, facilitates rapid identification of potential hit compounds. Integrating structure-based pharmacophore modelling with molecular dynamics (MD) simulations and docking enhances the predictive accuracy of binding interactions and ligand conformational stability. The present study employs a pharmacophoric approach in conjunction with complementary *in silico* methodologies to identify and optimise novel Fyn kinase inhibitors with improved efficacy.

Material and Methods

Pharmacophore hypothesis

The crystal structure of the Fyn kinase domain complexed with staurosporine, an inhibitor of kinase (PDB id - 2DQ7) was selected to develop a pharmacophore hypothesis. The pharmacophore model was generated employing key chemical features, including hydrogen bond acceptors, hydrogen bond donors, aromatic rings, and hydrophobic centres using the Pharmit server (https://pharmit.csb.pitt.edu/search.html)[16].

Screening of the database

The generated pharmacophore query was utilised on the Pharmit web server (http://pharmit.csb.pitt.edu)[17]. Virtual screening was conducted against the MolPort library, containing 6,482,4361 conformers from 4,742,020 molecules, which was updated on 05-09-2024 and used for screening.

Molecular property and ADMET filters

The pan assay interference compounds (PAINS), Lipinski's rule of five, were applied over the generated

hits. It was followed by filtration through parameters based on absorption, distribution, metabolism and excretion. Finally, the toxicity filters were applied to find suitable ligands for molecular docking studies. The filters were applied through Swiss ADME (http://www.swissadme.ch/index.php) and Deep-PK (https://biosig.lab.uq.edu.au/deeppk/)[18,19].

Protein preparation and validation

The crystal structures of human Fyn kinase were obtained from the protein databank (https://www.rcsb.org/) using Uniprot ID – P06241. The final structure was selected, and protonation states of the amino acid residues were determined through PDB2PQR server (https://server.poissonboltzmann.org/pdb2pqr) at physiological pH 7.4 using the AMBER force field 14SB for proteins. The hydrogen bond network of the protein was also optimised in this process. The resulting structure was subjected to energy minimisation using AMBER2022. The topology of the protein was prepared using the AMBER ff14SB force field. The final coordinate and topology files for the protein were generated using tleap. The system was solvated in a TIP3P water box under periodic boundary conditions, employing an 8 Å non-bonded cut-off and Particle Mesh Ewald (PME) method for long-range electrostatics. Energy minimisation was conducted using a convergence criterion with an RMS gradient threshold of 1×10^{-4} kcal/mol·Å through steepest descent and cojugate gradient algorithms (Suppl. Table 1). The protein obtained at the end of each stage was further validated using validation parameters such as QMEAN, Ramachandran plot and the MolProbity parameters[20-22].

Ligand preparation

The selected compounds were subjected to energy minimisation using General Amber Force Field (GAFF), RDKIT and Open Babel to optimise molecular geometry, eliminate steric clashes, and resolve atomic overlaps. The steepest descent algorithm was employed to locate the local energy minima by evaluating the total potential based on bonded and non-bonded interactions[23,24].

Identification of active site, grid generation and its validation

The active site of Fyn kinase was determined by studying protein-ligand interactions obtained from Discover Studio visualiser 2022. Further, the obtained residues generated a grid box around the active site. AutoGrid 4.0 was employed to create grid maps of interaction energies for various ligand atom types (A, C, HD, NA, N, OA, S, Br, Cl, and I). For staurosporine, the grid dimensions were set to 65 × 65 × 65 with a spacing of 0.375 Å. Grid validation was performed by redocking the ligand using randomised coordinates, and the resulting pose was assessed by calculating the RMSD of heavy atoms relative to the co-crystallised structure.

Molecular docking

The molecular docking was carried out in two stages using AutoDock 4.2. Initially, virtual screening was carried out, followed by precision docking of top-ranked compounds. The Lamarckian Genetic Algorithm (LGA) was utilised for conformational sampling in both phases, with parameter details provided in (Suppl. Table 2). Docking results were processed using vstools_v0.16, a Python-based utility. Post-docking analysis and visualisation were conducted using AutoDock Tools 1.5.6 and Discovery Studio Visualizer 2022, respectively.

Molecular dynamics studies

MD simulations were conducted to investigate the structural dynamics and stability of Fyn kinase and its complexes with selected ligands using AMBER2022. Each complex was solvated in a TIP3P water cubic box with a 12 Å buffer, and counter ions were added to neutralise the system. Long-range electrostatic interactions were treated using the PME method. The systems underwent energy minimisation, gradual heating, density equilibration and equilibration under periodic boundary conditions. The production phase of the simulation was carried out for 200 ns under an NPT ensemble at 310.15 K[25]. Visualisation of the 3D trajectories and molecular structures was performed using Visual Molecular Dynamics (VMD). The study was performed following the protocol previously reported[26].

Results and discussion

Pharmacophore hypothesis

Staurosporine is a kinase inhibitor exhibiting strong inhibition against Fyn kinase and binds to the ATP binding site. It has a bis-indole system comprising two indole rings fused to a central seven-membered ring, facilitating π interactions with protein residues. Its core structure is an indolocarbazole, a fused tricyclic system crucial for kinase inhibition. A lactam group in the central ring enables hydrogen bonding at the ATP-binding site. The oxygen atom of the 1,3,6-oxadiazepane ring also forms hydrogen bonds with amino acid residues (Fig. 1a).

Using these interactions, a pharmacophore map was prepared through the Pharmit server. The obtained pharmacophore map consists of two aromatic groups (A1 and A2), two hydrogen bond

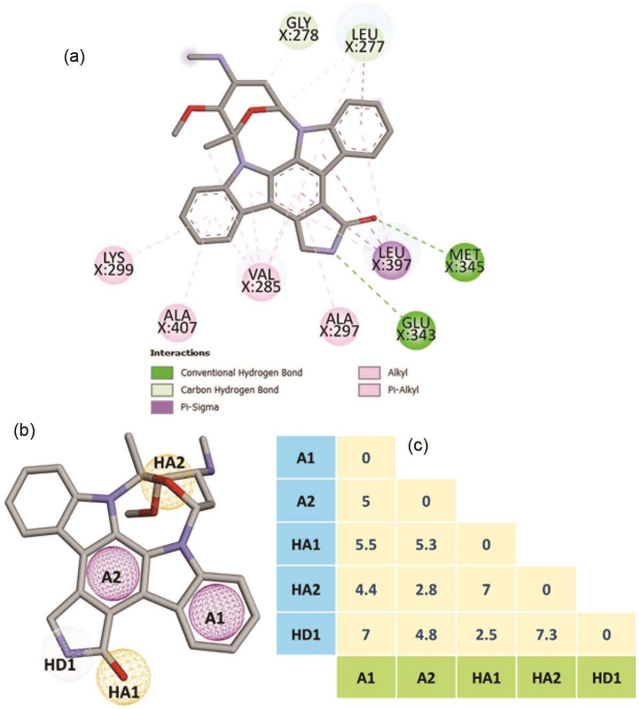


Fig. 1 — (a) 2D-interaction diagram of staurosporine complexed with Fyn kinase (PDB id – 2DQ7); (b) Pharmacophore mapping of staurosporine; and (c) Distance matrix depicting distances (in Å) between various pharmacophores

acceptors (HA1 and HA2), and one hydrogen bond donor (HD1) (Fig. 1b). The distances among the pharmacophore features are represented in (Fig. 1c).

Screening of the database

The generated pharmacophore model was employed to screen the MolPort database, comprising 64,824,361 conformers corresponding to 4,742,020 unique molecules (available as of 05/09/2024), using the Pharmit virtual screening platform. This process yielded 1,127 structurally diverse hit compounds, featuring a wide array of heterocyclic scaffolds such as thiazoles, benzothiazoles, piperazines, pyrazoles, and piperidines.

Molecular property and ADMET filters

Beginning with an initial pool of 1,127 virtual hit compounds, the application of Lipinski's Rule of Five, which evaluates drug-likeness through key physicochemical parameters predictive of oral bioavailability, alongside the Pan-Assay Interference Compounds (PAINS) filter, designed to eliminate false positives and non-specific binders, refined the dataset to 1,093 structurally suitable molecules. The subsequent application of a filter limiting the number of rotatable bonds to ten or fewer, a parameter linked to conformational rigidity and enhanced oral bioavailability, further reduced the candidate list to 1,081 compounds.

An *in silico* assessment of intestinal absorption, a critical determinant of oral pharmacokinetics, identified 1,066 compounds with predicted favourable absorption characteristics. Among these, 198 compounds were predicted to act as P-glycoprotein (P-gp) inhibitors, while 75 were identified as P-gp substrates. Given the central role of P-gp as an efflux transporter influencing drug bioavailability and central nervous system (CNS) penetration, these findings bear significance for optimising therapeutic exposure and minimising adverse drug-drug interactions.

From the remaining 793 compounds, a total of 562 molecules were predicted to possess blood–brain barrier permeability, a prerequisite for efficacious CNS-targeted therapeutics. Within this subset, 277 compounds exhibited inhibition of fewer than three cytochrome P450 (CYP) enzymes, suggesting a reduced likelihood of metabolic instability and cytochrome-mediated drug-drug interactions, thereby indicating improved pharmacokinetic viability.

Subsequent toxicity profiling of these 277 compounds revealed that 119 were non-mutagenic based on the Ames test, 111 were predicted to be non-carcinogenic, and 104 did not exhibit inhibitory activity against the human Ether-à-go-go-Related Gene (hERG) potassium channel, a key indicator for assessing cardiotoxicity. These cumulative filtration steps constitute a scientifically robust strategy for prioritising CNS-permeable compounds with favourable pharmacokinetic and toxicological attributes, suitable for advancement in drug discovery pipelines (Tables 1 & 2, and Suppl. Table 1).

Protein preparation and validation

The initial protein structure (PDB ID: 2DQ7) was refined using the PDB2PQR server, which enabled structural preparation at physiological pH 7.4. This step added missing atoms, standardised nomenclature, and assigned atomic radii and partial charges according to the AMBER force field. The PROPKA utility was employed to assign the correct protonation states of ionisable residues, which is critical for accurate molecular docking and virtual screening, as the protonation state significantly influences residue charge distribution and thereby the ligand-binding landscape. Eight sequential stages were executed for energy minimisation (Suppl. Table 1). The initial potential energy of the system was −102540.6

Table 1 — Molecular properties of selected compounds

Compound ID	Molecular weight	Log(P)	Hydrogen bond acceptor	Hydrogen bond donor	Lipinski Violation	Rotatable bonds	pKa Acid
MolPort-000-414-107	345.387	4.01	7	2	0	3	8.59
MolPort-005-915-880	442.504	2.78	6	3	0	3	9.95
MolPort-005-914-867	426.436	1.77	6	3	0	3	10.15
MolPort-003-049-507	409.833	3.52	6	2	0	5	10.1
MolPort-003-049-585	440.257	3.47	6	3	0	3	8.67
MolPort-023-306-537	411.465	3.85	5	2	0	3	10.11
MolPort-003-049-539	460.675	3.71	6	3	0	3	8.04
MolPort-005-912-438	427.42	2.61	7	2	0	3	10.3
MolPort-023-306-533	394.394	2.09	6	2	0	2	10.01
MolPort-005-916-947	448.28	3.38	5	2	0	2	9.97

Table 2 — ADME properties of selected compounds

Compound ID	Human Intestinal Absorption	P-Glycoprotein Inhibitor	P-Glycoprotein Substrate	Blood-Brain Barrie	CYP 1A2 Inhibitor	CYP 2C19 Inhibitor	CYP 2C9 Inhibitor	CYP 2D6 Inhibitor	CYP 3A4 Inhibitor
MolPort-000-414-107	Absorbed	Non-Inhibitor	Non-Substrate	Penetrable	Inhibitor	Non-Inhibitor	Inhibitor	Non-Inhibitor	Non-Inhibitor
MolPort-005-915-880	Absorbed	Non-Inhibitor	Non-Substrate	Penetrable	Non-Inhibitor	Inhibitor	Inhibitor	Non-Inhibitor	Non-Inhibitor
MolPort-005-914-867	Absorbed	Non-Inhibitor	Non-Substrate	Penetrable	Non-Inhibitor	Inhibitor	Inhibitor	Non-Inhibitor	Non-Inhibitor
MolPort-003-049-507	Absorbed	Non-Inhibitor	Non-Substrate	Penetrable	Inhibitor	Inhibitor	Non-Inhibitor	Non-Inhibitor	Non-Inhibitor
MolPort-003-049-585	Absorbed	Non-Inhibitor	Non-Substrate	Penetrable	Inhibitor	Inhibitor	Non-Inhibitor	Non-Inhibitor	Non-Inhibitor
MolPort-023-306-537	Absorbed	Non-Inhibitor	Non-Substrate	Penetrable	Non-Inhibitor	Inhibitor	Inhibitor	Non-Inhibitor	Non-Inhibitor
MolPort-003-049-539	Absorbed	Non-Inhibitor	Non-Substrate	Penetrable	Inhibitor	Inhibitor	Non-Inhibitor	Non-Inhibitor	Non-Inhibitor
MolPort-005-912-438	Absorbed	Non-Inhibitor	Non-Substrate	Penetrable	Non-Inhibitor	Inhibitor	Inhibitor	Non-Inhibitor	Non-Inhibitor
MolPort-023-306-533	Absorbed	Non-Inhibitor	Non-Substrate	Penetrable	Non-Inhibitor	Non-Inhibitor	Inhibitor	Non-Inhibitor	Non-Inhibitor
MolPort-005-916-947	Absorbed	Non-Inhibitor	Non-Substrate	Penetrable	Non-Inhibitor	Inhibitor	Inhibitor	Non-Inhibitor	Non-Inhibitor

kcal/mol, which was dramatically reduced to −179070.4 kcal/mol after the final stage, yielding a net decrease of 76529.8 kcal/mol. The highest energy reduction was observed during Stage 1, indicating the release of substantial steric strain and conformational tension from the initial structure. This was reflected by the largest energy decrease of −65,180.1 kcal/mol and a mean gradient of −13.0360 kcal/mol/step. Subsequent stages (2–4) contributed to moderate and then diminishing energy reductions, suggesting a transition from high-gradient steepest descent minimisation to gentler convergence as the system approached a local minimum. In the final stages (Stages 5–8), energy changes were minimal (Stage 8: −15.2 kcal/mol with a mean gradient of −0.0061 kcal/mol/step), indicating that the protein structure had reached a stable low-energy conformation with minimal atomic fluctuations (Fig. 2).

The structural refinement was validated using MolProbity and Ramachandran plot analyses. Although the MolProbity score initially worsened due to transient clashes (Stage 1: 3.49), it improved steadily to 1.45 by Stage 8. Clash scores were significantly reduced from 43.59 to 0.48, indicating successful resolution of steric overlaps. Ramachandran favoured residues increased from 86.59% to 92.74%, with outliers and rotamer issues markedly minimised. Minor bond geometry deviations observed in early stages were fully corrected by Stage 6. The QMEAN score remained stable (0.84–0.86), confirming consistent global model quality throughout the minimisation process

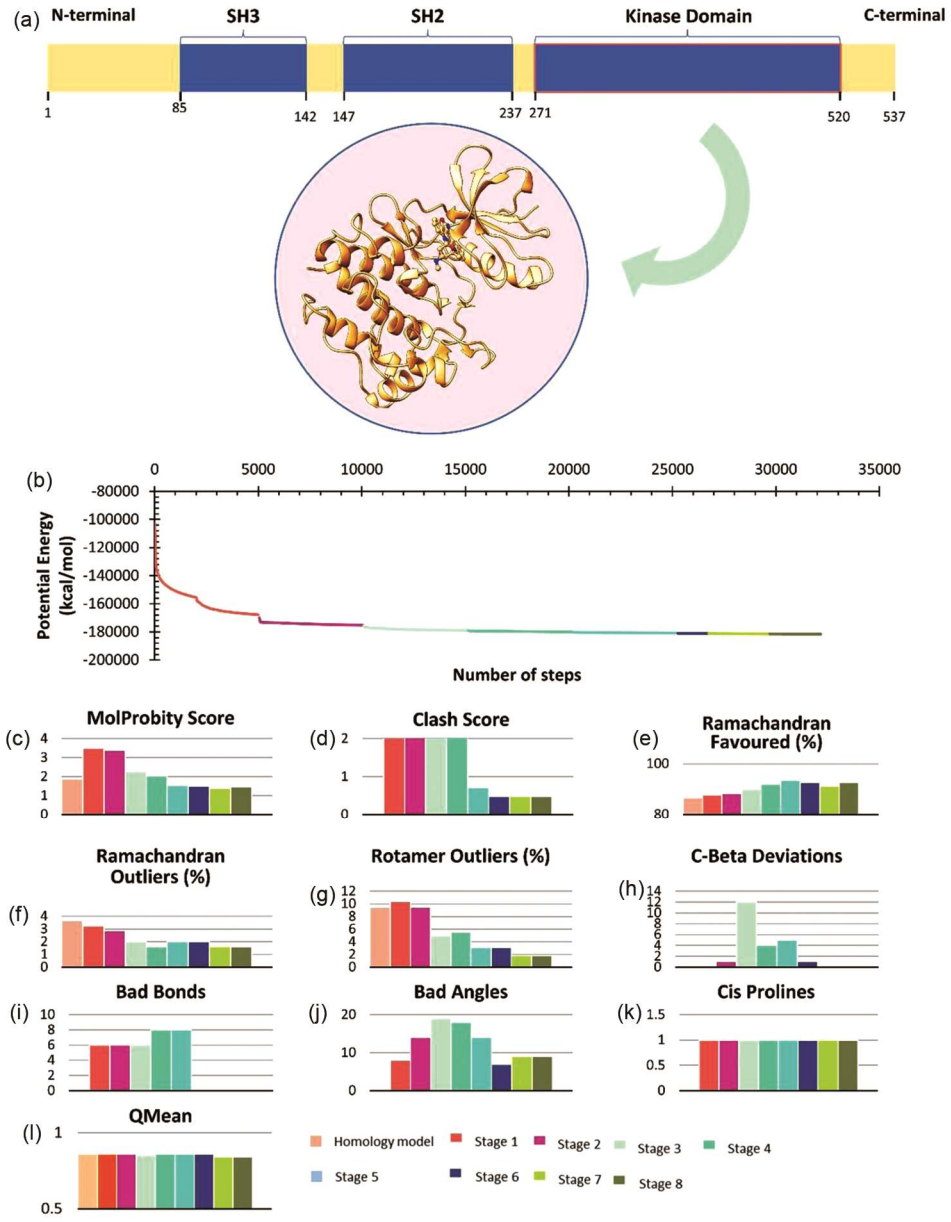


Fig. 2 — (a) Representation of the Fyn kinase domain and ATP binding site; (b) Potential energy changes (kcal/mol) in protein models during minimisation; and (c – l) Validation scores of protein models during energy minimisation

(Fig. 2). The generated PDB file, at the end of the minimisation process, was subsequently converted to the PDBQT format required for AutoDock 4.2.

Ligand preparation

The energy minimisation of the compounds was carried out using RDKIT and Open Babel to correct geometrical distortions and eliminate steric clashes. The steepest descent algorithm was employed to locate a local energy minimum based on bonded and non-bonded interactions.

Identification of active site, grid generation and its validation

The interaction analysis of staurosporine with Fyn kinase revealed a combination of hydrogen bonding and extensive hydrophobic interactions, contributing to its stable binding conformation. Two key conventional hydrogen bonds were observed: one between Met345 and staurosporine, and another between STU902 and the carboxylate oxygen of Glu343. Additional carbon-hydrogen bonds involved Gly278 and Leu277. Notably, staurosporine engaged in multiple hydrophobic contacts, including π-σ

interactions with Leu277 and Leu397, and several π-alkyl interactions with residues such as Val285, Ala297, Leu277, Lys299, and Ala407. These interactions suggest a strong affinity and effective stabilisation of staurosporine within the Fyn kinase binding site (Fig. 1a).

Autogrid4 was used to generate pre-calculated atomic affinity potentials, enhancing the computational efficiency of the docking procedure. The grid box dimensions and point spacing were validated, ensuring the docking protocol's accuracy by reproducing the co-crystallised ligand pose with minimal deviation. The selected grid parameters demonstrated acceptable RMSD deviations of 1.67 Å within the acceptable limit of 2 Å. These results confirm the grid's reliability for virtual screening and precision docking (Fig. 3).

Molecular docking

During the virtual screening, out of 104 compounds and the reference ligand staurosporine, 11 top-ranking candidates were shortlisted based on the 10th percentile binding energy threshold. These selected compounds exhibited binding affinities ranging from −9.72 to −9.03 kcal/mol. The overall docking results showed a near-normal distribution of binding energies, with the majority of compounds clustering around moderately high affinities (Suppl. Table 4). Only compounds achieving the top 10 percentile cut-off were considered for further precision docking to ensure focused evaluation of the most promising hits (Fig. 3).

Precision molecular docking was carried out utilising the extended LGA, with a population size set at 100 to enhance the efficiency of conformational sampling. To ensure reliability in pose prediction, clustering analysis was implemented with a RMSD tolerance of 2 Å, and only clusters comprising 50 or more conformers were considered for further evaluation, thereby prioritising ligands with both favourable binding energies and conformational stability (Table 3).

Among the screened molecules, two compounds demonstrated significant clustering and were shortlisted for detailed analysis. Staurosporine, a well-characterised kinase inhibitor, served as the reference compound and exhibited the most favourable binding energy of −9.86 kcal/mol, with a cluster size of 41

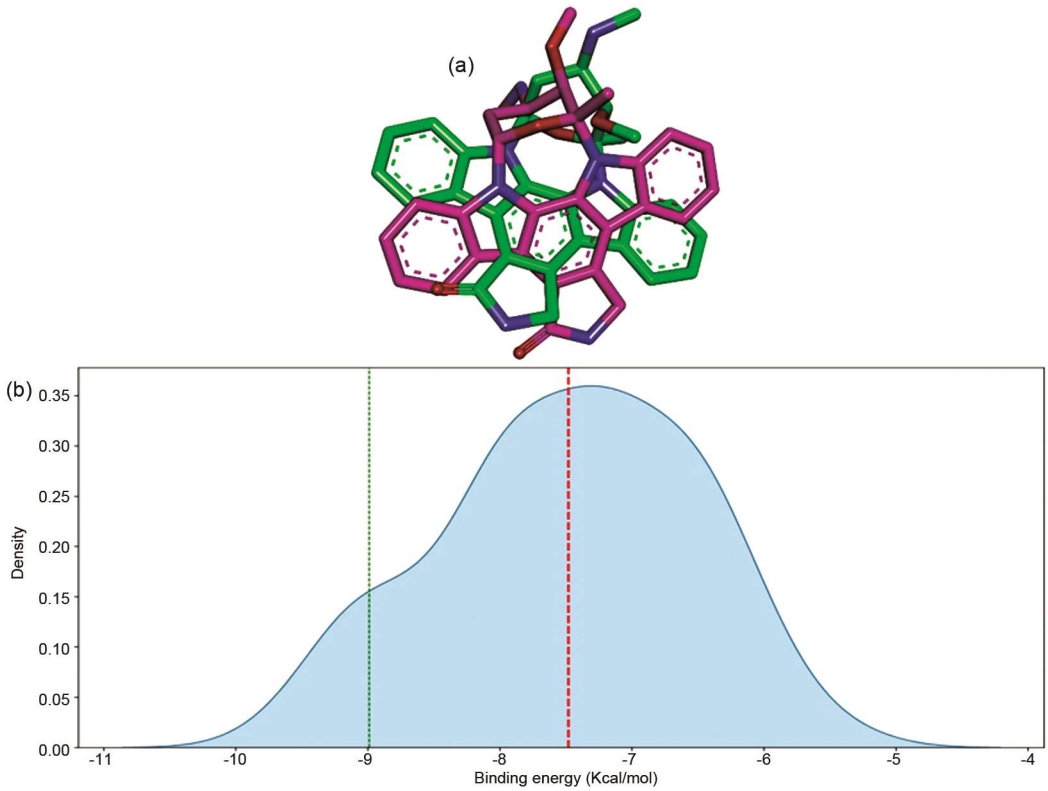


Fig. 3 — (a) Superimposition of docked (magenta) with co-crystallised (green) structures of staurosporine; and (b) Distribution of binding energies of ligands during virtual screening (red broken line represents the mean of population and green broken line represents the 10th percentile

Table 3 — Binding energy of selected compounds obtained through precision docking.

Compound ID	Lowest binding energy (Kcal/mol)	Mean binding energy (kcal/mol)	Cluster size
Staurosporine	-9.86	-9.65 ± 0.23	41
MolPort-000-414-107	-9.59	-9.47 ± 0.094	89
MolPort-005-915-880	-9.52	-9.45 ± 0.053	85
MolPort-005-914-867	-9.44	-9.27 ± 0.07	63
MolPort-003-049-507	-9.56	-9.13 ± 0.397	30
MolPort-003-049-585	-9.39	-9.1 ± 0.411	73
MolPort-023-306-537	-9.74	-9.45 ± 0.011	48
MolPort-003-049-539	-9.25	-8.94 ± 0.442	45
MolPort-005-912-438	-9.2	-9.11 ± 0.097	65
MolPort-023-306-533	-9.2	-9.1 ± 0.82	58
MolPort-005-916-947	-9.12	-9.04 ± 0.0352	65

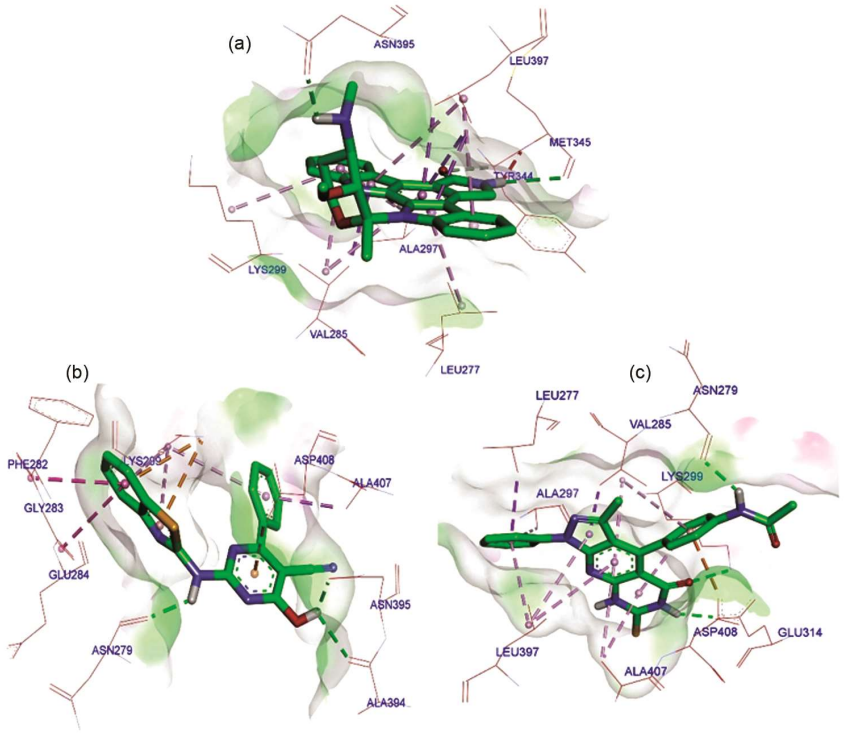


Fig. 4 — 3D interaction diagram of (a) staurosporine; (b) with MolPort-000-414-107; and (c) MolPort-005-915-880 with Fyn kinase (PDB id – 2DQ7)

and a mean binding energy of −9.65 ± 0.23 kcal/mol. The docking profile indicated the formation of conventional hydrogen bonds with residues Asn395 and Met345, along with a carbon-hydrogen bond involving Tyr344. Additionally, the ligand engaged in multiple π–σ interactions with Val285 and Leu397, and a network of π–alkyl interactions with Ala297, Leu397, Leu277, Val285, and Lys299, highlighting a robust hydrophobic anchoring within the receptor's binding pocket (Fig. 4).

MolPort-000-414-107 displayed a minimum binding energy of −9.59 kcal/mol and a mean binding energy of −9.47 ± 0.094 kcal/mol, forming a dominant cluster with 89 conformations. It formed three conventional hydrogen bonds with Ala394, Asn395, and Asn279. It also participated in non-covalent interactions, including π–cation bonding with Lys299 and π–anion bonding with Asp408. Hydrophobic interactions included π–σ contacts with Ala407, amide–π stacking with Phe282, Gly283, and Glu284, and extensive π–alkyl interactions predominantly involving LYS299. MolPort-005-915-880 was the second most promising candidate, showing a minimum binding energy of −9.52 kcal/mol and a mean of −9.45 ± 0.053 kcal/mol with a cluster size of 85. The ligand formed three

conventional hydrogen bonds with Lys299, Glu314, and Asn279. Additionally, it engaged in π–anion interactions with Asp408 and exhibited numerous hydrophobic contacts, including π–σ interactions with Leu277 and Val285, as well as π–alkyl interactions with Leu397, Ala407, Lys299, Val285, and Ala297 (Fig. 4). The interaction profiles of staurosporine and the two lead compounds revealed strong and diverse binding interactions, involving both polar and nonpolar residues.

Molecular dynamics studies

MD simulations represent a state-of-the-art approach for investigating the temporal evolution and conformational behaviour of biomolecular systems, enabling the detailed examination of atomic motions and intermolecular interactions under physiological conditions.

Root Mean Square Deviation

RMSD quantifies the average positional deviations of atoms in a structure over time relative to a reference conformation, typically the initial frame. Lower RMSD values indicate greater structural stability throughout the simulation.

In the present study, we analysed RMSD values for the apo form of Fyn kinase and its complexes with MolPort-000-414-107 and MolPort-005-915-880 over a 200 ns simulation. The RMSD fluctuations ranged between 1–3 Å, a range generally considered acceptable for globular proteins, reflecting stable dynamics. The average RMSD for the apo protein was 2.34 ± 0.29 Å. In contrast, Fyn kinase complexes with ligands MolPort-000-414-107 and MolPort-005-915-880 exhibited mean RMSD values of 2.12 ± 0.27 and 1.87 ± 0.2 Å, respectively. These results indicated conformational stability upon ligand binding, with the least deviation, suggesting superior structural integrity among all tested ligands (Fig. 5).

Furthermore, we calculated the mean RMSD deviations of the ligands within the enzyme cavity, which were 1.36 ± 0.18 and 0.86 ± 0.19 Å for MolPort-000-414-107 and MolPort-005-915-880, respectively. The end point RMSD was 1.40, and 0.94 Å for MolPort-000-414-107 and MolPort-005-915-880, respectively. These findings suggest that all ligands bound stably. Notably, the average and endpoint RMSD values differed little across all systems, confirming that the ligand-bound complexes reached stable conformations by the end of the simulation (Fig. 5).

Root Mean Square Fluctuation

The Root Mean Square Fluctuation (RMSF) analysis provides insight into local flexibility and mobility of amino acid residues within the protein structure throughout the MD simulation. Lower RMSF values typically reflect regions of structural rigidity or stabilisation, often as a consequence of ligand binding. The RMSF values were computed for the protein 2DQ7 in its apo form and in complex with two different ligands—MolPort-000-414-107 and MolPort-005-915-880. A general reduction in RMSF values across a majority of residues was observed upon ligand binding, particularly with residues 261–278. This suggests a stabilising interaction of the ligand with these regions, which may contribute to the overall structural integrity of the protein-ligand complex. Further, the stabilisation was observed in residues 354 – 359 and 416 – 426 upon ligand binding. In the case of atomic fluctuation of MolPort-000-414-107, the phenyl ring attached to pyrimidine was found to be more flexible. This might be because it displayed a minimal and weak hydrophobic interaction with Lys299 and Ala407. MolPort-005-915-880 displayed higher fluctuation in the phenyl ring attached to pyrazole. The reason for fluctation was minimal interaction with Leu277, Ala297 and Leu397 through hydrophobic contact (Fig. 5).

Radius of gyration

The radius of gyration (Rg) analysis over a 200 ns simulation period reveals dynamic structural stability differences among the apo protein (2DQ7) and its complexes with MolPort-000-414-107 and MolPort-005-915-880. The mean Rg was 19.52 ± 016, 19.45 ± 0.25 and 19.29 ± 0.19 Å for apo protein and its complexes with MolPort-000-414-107 and MolPort-005-915-880, respectively. The apo form consistently maintained an Rg value in the narrow range of 18.99 - 20.05 Å, indicative of a relatively stable and compact conformation throughout the simulation. Both ligand did not significantly influenced the compactness or structural dynamics of the protein (Fig. 6).

The Rg analysis revealed that both ligands maintained stable conformational behaviour throughout the simulation period. MolPort-000-414-107 exhibited a mean Rg of 3 ± 0.05 Å, ranging from 3.77 to 4. Å. Similarly, MolPort-005-915-880 showed a slightly higher mean Rg of 4.57 ± 0.03 Å, and values ranging from 4.43 to 4.Å. These results indicate that

neither ligand underwent significant conformational fluctuations, suggesting a consistent and compact structural profile during the simulation (Fig. 6).

Solvent accessible surface area

The Solvent Accessible Surface Area (SASA) analysis revealed notable differences between the unbound protein and its ligand-bound complexes. The native protein (2DQ7) exhibited a mean SASA of 14152.68 ± 366.67 Å². Upon binding with MolPort-000-414-107, the mean SASA was reduced to 13753.92 ± 358.35 Å², while the 2DQ7–MolPort-005-915-880 complex demonstrated a further decrease to

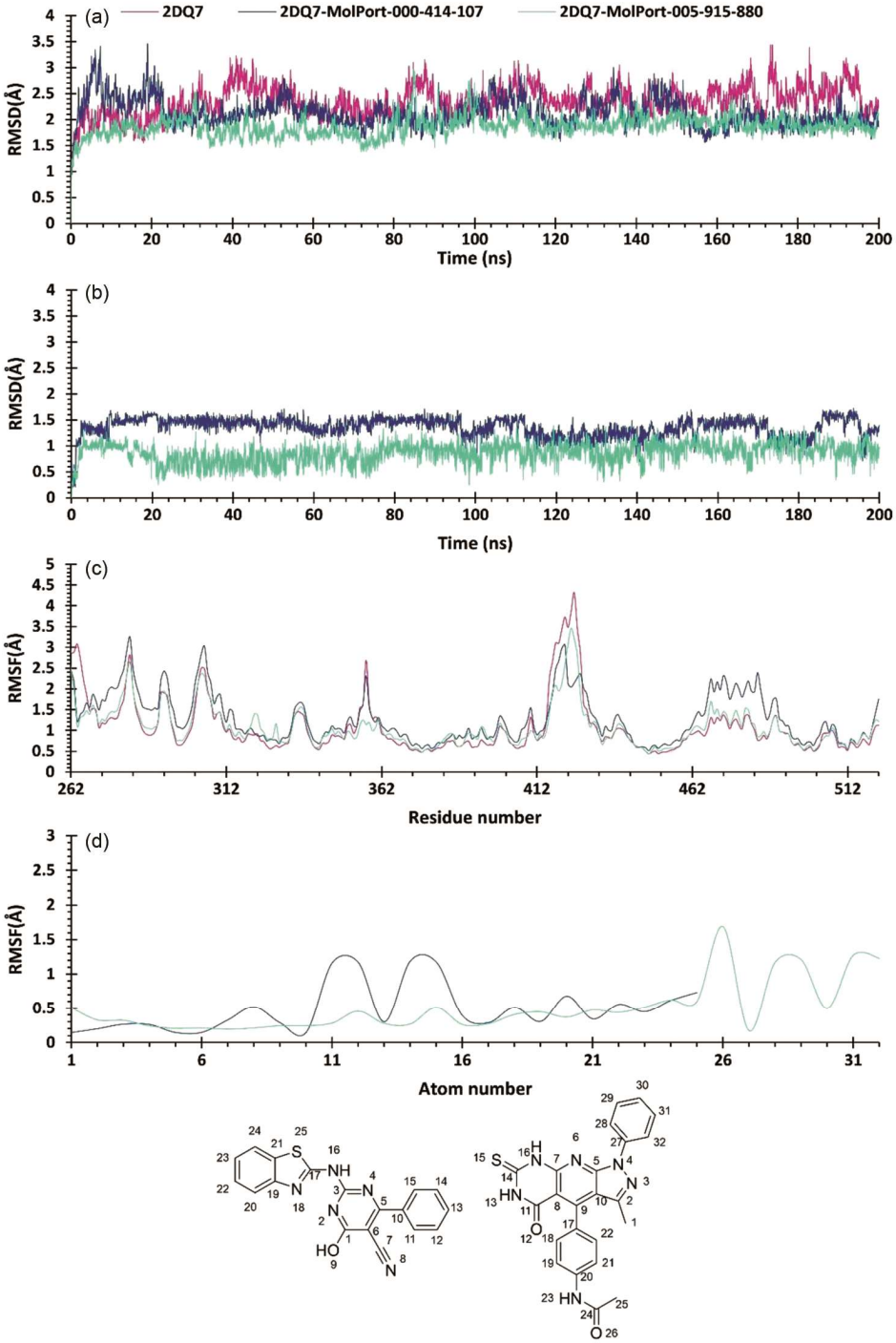


Fig. 5 — RMSD plot of (a) protein-ligand complexes; and (b) ligands. RMSF plot of (c) protein-ligand complexes; and (d) ligands

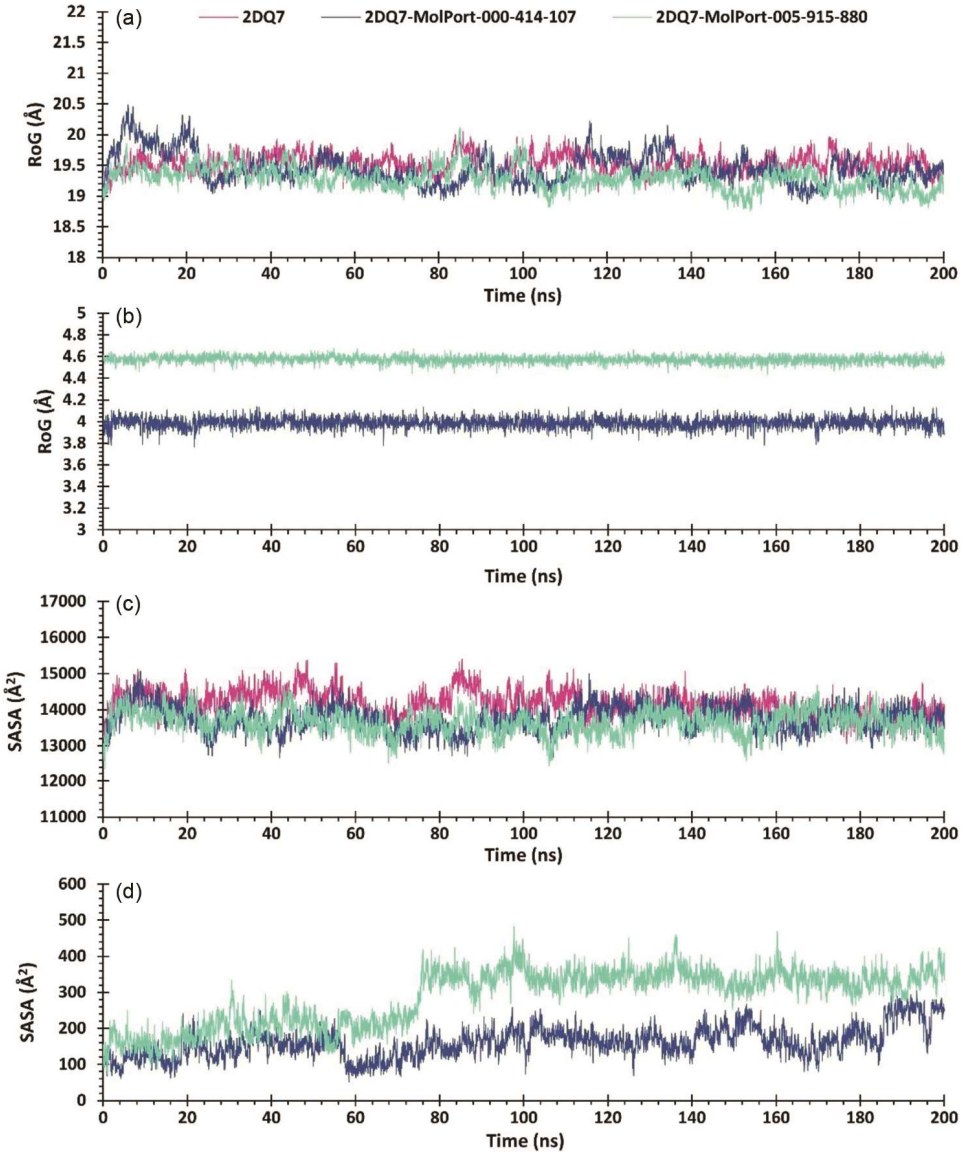


Fig. 6 — RoG of (a) protein-ligand complexes; and (b) ligands. SASA plot of (c) protein-ligand complexes; and (d) ligands

13652.27 ± 330.19 Å². This progressive reduction in SASA values upon ligand binding indicates a slight compaction of the protein structure, reflecting decreased solvent accessibility and suggesting potential stabilisation of the protein conformation in the ligand-bound states (Fig. 6).

The SASA analysis of the ligands in their bound states revealed distinct differences in their exposure to the solvent environment. MolPort-000-414-107 exhibited a SASA of 161.28 ± 42.75 Å², while MolPort-005-915-880 showed a significantly higher SASA of 287.45 ± 77.48 Å². These findings indicate that MolPort-005-915-880 remains more solvent-exposed during the simulation, which may reflect differences in their binding orientation, flexibility, or extent of burial within the protein binding pocket (Fig. 6).

Hydrogen bond analysis

Hydrogen bond analysis over the 200 ns molecular dynamics simulations revealed that MolPort-000-414-107 and MolPort-005-915-880 engage distinct yet complementary interactions within the binding pocket. MolPort-000-414-107 formed its most persistent hydrogen bond with Asp408 (28.05% of contact time), followed by Ser349 (23.33%) and Met345 (18.98%), with only sporadic contacts observed for Leu277 (3.40%), Lys299 (1.80%), and Asn279 (1.45%), and marginal involvement of

Tyr344, Ala394, Ile396, and Thr342 (< 0.5% each). In contrast, MolPort-005-915-880 exhibited a markedly higher reliance on polar side chains, with Ser349 and Thr342 dominating its hydrogen-bonding profile (59.10% and 45.25% occupancy, respectively), supplemented by moderate stabilisation *via* Lys299 (15.08%), Lys275 (13.15%), and Lys302 (10.70%), and occasional interactions with Phe282 (6.53%) and Phe409 (6.28%). These complementary interaction patterns suggest that while MolPort-000-414-107 relies on a broader distribution of contacts, particularly with charged and polar residues, MolPort-005-915-880 achieves greater binding persistence through a focused engagement of serine and threonine residues, underscoring differences in their binding modes and potential affinities (Fig. 7).

MM-GBSA

Free energy calculations using MM-GBSA are widely employed to estimate ligand binding affinities by evaluating molecular interactions within protein–ligand complexes. These methods decompose binding energy ($\Delta G_{binding}$) into gas-phase energy (ΔG_{gas}) and solvation energy (ΔG_{sol}). ΔG_{gas} includes bonded (bond, angle, dihedral) and non-bonded (van der Waals, electrostatic) terms, while ΔG_{sol} comprises polar (*via* GB models) and non-polar (via SASA) contributions.

The MM-GBSA free energy calculations for both ligands, MolPort-000-414-107 and MolPort-005-915-880, suggest favourable binding affinities with the protein target. MolPort-000-414-107 exhibited a binding free energy (ΔG_{total}) of –23.62 kcal/mol, predominantly driven by van der Waals

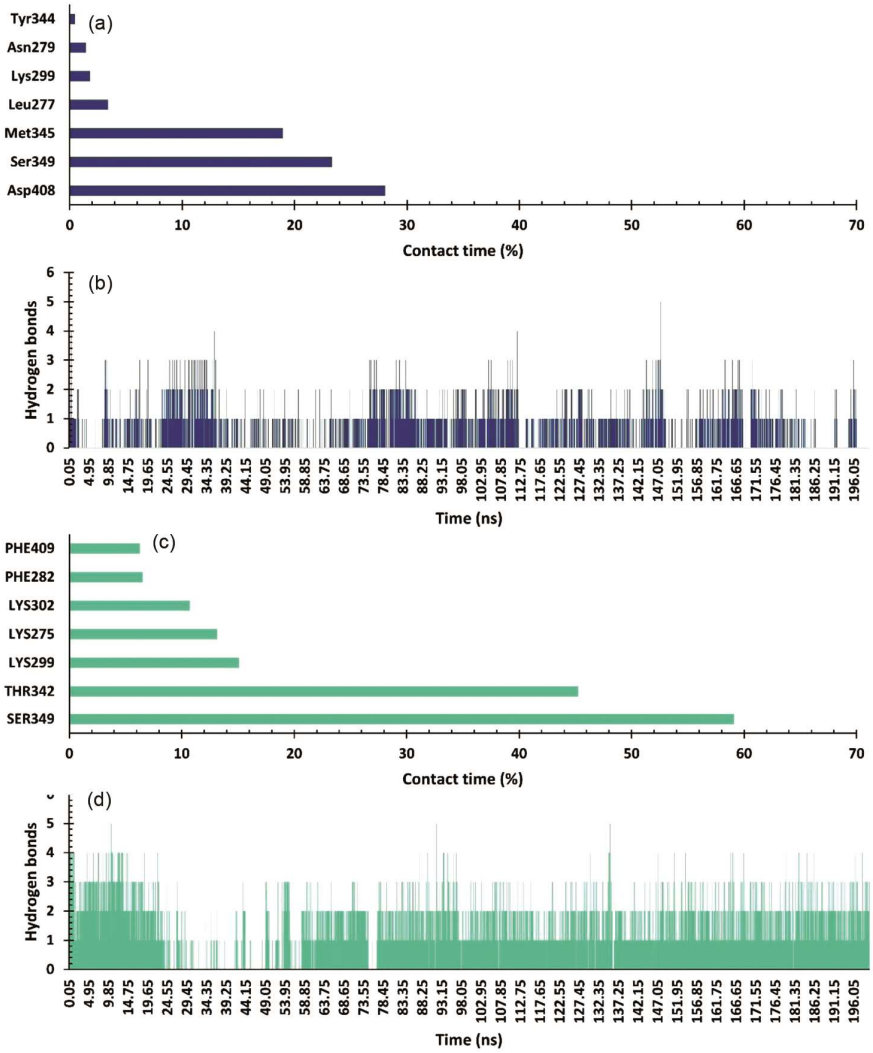


Fig. 7 — (a) Contact time (%) with residues; (b) Hydrogen bond contact of MolPort-000-414-107 with Fyn kinase; (c) Contact time (%) with residues; and (d) Hydrogen bond contact of MolPort-005-915-880 with Fyn kinase

Table 4 — Energy contribution of ligands in MM-GBSA

Compound ID	ΔE_{vdw}	ΔE_{ele}	ΔG_{GB}	$\Delta G_{Nonpolar}$	$\Delta G_{MM\text{-}GBSA}$
MolPort-000-414-107	-34.3236 ± 0.9185	-9.3782 ± 1.5356	24.1549 ± 1.5306	-4.0692 ± 0.2047	-23.6162 ± 0.9311
MolPort-005-915-880	-26.5676 ± 0.9643	-49.5031 ± 2.5578	61.1177 ± 2.3302	-3.5234 ± 0.0731	-18.4764 ± 0.7379

(–34.32 kcal/mol) and electrostatic (–9.38 kcal/mol) interactions, partially offset by solvation effects (+20.09 kcal/mol). Conversely, MolPort-005-915-880 displayed a slightly less negative ΔG_{total} of –18.48 kcal/mol, despite stronger electrostatic contributions (–49.50 kcal/mol), as the high polar solvation energy (+61.12 kcal/mol) counteracted favourable gas-phase interactions. Overall, both ligands showed energetically favourable binding, with MolPort-000-414-107 exhibiting a more balanced interaction profile, suggesting slightly superior binding stability under the simulation conditions (Table 4).

Conclusion

The pharmacophore model derived from the Fyn kinase inhibitor staurosporine, featuring two aromatic groups, two hydrogen bond acceptors, and one hydrogen bond donor, successfully screened a large database, yielding 1,127 initial hits. Subsequent *in silico* filtering based on Lipinski's Rule of Five, PAINS, rotatable bonds, intestinal absorption, P-gp modulation, blood-brain barrier permeability, CYP inhibition, and toxicity profiles progressively narrowed the selection to 104 non-mutagenic, non-carcinogenic compounds without hERG inhibition and predicted CNS permeability. Molecular docking studies of the top 11 virtual screening hits against Fyn kinase revealed two promising lead compounds, MolPort-000-414-107 and MolPort-005-915-880, exhibiting comparable binding energies and significant cluster sizes to the reference inhibitor staurosporine. These compounds demonstrated strong interactions within the ATP-binding site, including hydrogen bonds, π-cation, π-anion, and hydrophobic interactions with key residues like Asn395, Lys299, and Asp408. MD simulations over 200 ns confirmed the stability of Fyn kinase in complex with both lead compounds, MolPort-000-414-107 and MolPort-005-915-880, as evidenced by acceptable RMSD and Rg values. Ligand binding generally reduced protein flexibility (RMSF) and solvent accessibility (SASA). Hydrogen bond analysis revealed distinct interaction patterns for each ligand. MM-GBSA calculations indicated favorable binding free energies for both compounds, with MolPort-000-414-107 exhibiting a slightly more balanced energy profile. These findings reinforce the potential of both compounds as Fyn kinase inhibitors.

Acknowledgement

The authors would also like to extend their gratitude toward Professor David A. Case, Department of Chemistry & Chemical Biology, Rutgers University, New Jersey, USA, for granting a license for Amber 2022. The support and the resources provided by the'PARAM BRAHMA FACILITY' under the National Supercomputing Mission, Government of India at the IISER, Pune are gratefully acknowledged.

Conflict of interest

All authors declare no conflict of interest.

References

1 Hubbard SR & Till JH, Protein tyrosine kinase structure and function. *Annu Rev Biochem*, 69 (2000) 373.

2 Paul MK & Mukhopadhyay AK, Tyrosine kinase–role and significance in cancer. *Int J Med Sci*, 1 (2004) 101.

3 Lamers MB, Antson AA, Hubbard RE, Scott RK & Williams DH, Structure of the protein tyrosine kinase domain of C-terminal Src kinase (CSK) in complex with staurosporine. *J Mol Biol*, 285 (1999) 713.

4 Peng S & Fu Y, FYN: emerging biological roles and potential therapeutic targets in cancer. *J Transl Med*, 21 (2023) 84.

5 Grabulovski D & Bertschinger J, Scaffolds: Small globular proteins as antibody substitutes, in *Drug Discovery and Development* (Second Edition), edited by RG Hill & HP Rang (Churchill Livingstone) 2013, 189

6 Kinoshita T, Matsubara M, Ishiguro H, Okita K & Tada T, Structure of human Fyn kinase domain complexed with staurosporine. *Biochem Biophys Res Commun*, 346 (2006) 840.

7 Omura S, Iwai Y, Hirano A, Nakagawa A, Awaya J, Tsuchiya H, Takahashi Y & Masuma R, A new alkaloid AM-2282 of Streptomyces origin: taxonomy, fermentation, isolation and preliminary characterization. *J Antibiot*, 30 (1977) 275.

8 Nakano H, Kobayashi E, Takahashi I, Tamaoki T, Kuzuu Y & Iba H, Staurosporine inhibits tyrosine-specific protein kinase activity of Rous sarcoma virus transforming protein p60. *J Antibiot*, 40 (1987) 706.

9 Tamaoki T, Nomoto H, Takahashi I, Kato Y, Morimoto M & Tomita F, Staurosporine, a potent inhibitor of phospholipid/Ca++ dependent protein kinase. *Biochem Biophys Res Commun*, 135 (1986) 397.

10 Meggio F, Deana AD, Ruzzene M, Brunati AM, Cesaro L, Guerra B, Meyer T, Mett H, Fabbro D & Furet P, Different susceptibility of protein kinases to staurosporine inhibition: kinetic studies and molecular bases for the resistance of protein kinase CK2. *Eur J Biochem*, 234 (1995) 317.
11 Cozza G & Pinna LA, Casein kinases as potential therapeutic targets. *Expert Opin Ther Targets*, 20 (2016) 319.
12 Nygaard HB, van Dyck CH & Strittmatter SM, Fyn kinase inhibition as a novel therapy for Alzheimer's disease. *Alzheimers Res Ther*, 6 (2014) 8.
13. Meur S & Karati D, Fyn kinase in Alzheimer's disease: unraveling molecular mechanisms and therapeutic implications. *Mol Neurobiol*, 62 (2025) 643.
13 Engin AB & Engin A, Alzheimer's disease and protein kinases, in *Protein Kinase-Mediated Decisions Between Life and Death* (Springer Cham, Switzerland) 2021, 285.
14 Nygaard HB, Targeting Fyn kinase in Alzheimer's disease. *Biol Psychiatry*, 83 (2018) 369.
15 Koes DR, The Pharmit backend: a computer systems approach to enabling interactive online drug discovery. IBM *J Res Dev*, 62 (2018) 3.
16 Sunseri J & Koes DR, Pharmit: interactive exploration of chemical space. *Nucleic Acids Res*, 44 (2016) W442.
17 Daina A, Michielin O & Zoete V, SwissADME: a free web tool to evaluate pharmacokinetics, drug-likeness and medicinal chemistry friendliness of small molecules. *Sci Rep*, 7 (2017) 42717.
18 Myung Y, de Sá AG & Ascher DB, Deep-PK: deep learning for small molecule pharmacokinetic and toxicity prediction. *Nucleic Acids Res*, 52 (2024) W469.
19 Ganeshpurkar A, Singh R, Kumar D, Gutti G, Sardana D, Shivhare S, Bhushan Singh R, Kumar A & Singh SK, Development of homology model, docking protocol and machine-learning based scoring functions for identification of Equus caballus's butyrylcholinesterase inhibitors. *J Biomol Struct Dyn*, 40 (2022) 13693.
20 Ganeshpurkar A, Singh R, Gore PG, Kumar D, Gutti G, Kumar A & Shivhare S, Structure-based screening and molecular dynamics simulation studies for the identification of potential acetylcholinesterase inhibitors. *Mol Simul*, 46 (2020) 169.
21 Chen VB, Arendall WB, Headd JJ, Keedy DA, Immormino RM, Kapral GJ, Murray LW, Richardson JS & Richardson DC, MolProbity: all-atom structure validation for macromolecular crystallography. *Acta Crystallogr D Biol Crystallogr*, 66 (2010) 12.
22 Bento AP, Hersey A, Félix E, Landrum G, Gaulton A, Atkinson F, Bellis LJ, De Veij M & Leach AR, An open source chemical structure curation pipeline using RDKit. *J Cheminform*, 12 (2020) 51.
23 O'Boyle NM, Banck M, James CA, Morley C, Vandermeersch T & Hutchison GR, Open Babel: an open chemical toolbox. *J Cheminform*, 3 (2011) 1.
24 Case DA, Aktulga HM, Belfon K, Cerutti DS, Cisneros GA, Cruzeiro VWD, Forouzesh N, Giese TJ, Götz AW, Gohlke H, Izadi S, Kasavajhala K, Kaymak MC, King E, Kurtzman T, Lee TS, Li P, Liu J, Luchko T, Luo R, Manathunga M, Machado MR, Nguyen HM, O'Hearn KA, Onufriev A, Pan F, Pantano S, Qi R, Rahnamoun A, Risheh A, Schott-Verdugo S, Shajan A, Swails J, Wang J, Wei H, Wu X, Wu Y, Zhang S, Zhao S, Zhu Q, Cheatham TE, Roe DR, Roitberg A, Simmerling C, York DM, Nagan MC & Merz KM, AmberTools. *J Chem Inf Model*, 63 (2023) 6183.
25 Ganeshpurkar A, Singh R, Kumar D, Divya, Shivhare S, Kumar A & Singh SK, Computational binding study with α7 nicotinic acetylcholine receptor of Anvylic-3288: an allosteric modulator. *Mol Simul*, 46 (2020) 975.